KSCE Journal of Civil Engineering (0000) 00(0):1-8
DOI 10.1007/s12205-018-1367-x

Structural Engineering
pISSN 1226-7988, eISSN 1976-3808
www.springer.com/12205

Method for Evaluating Damage Caused to Steel Columns by Local Buckling

Yeon-Soo Park* and Dae-Hung Kang**

Received September 10, 2017/Revised November 8, 2017/Accepted December 6, 2017/Published Online February 5, 2018

Abstract

In this study the process by which a steel column subjected to strong and repeated loading undergoes failure is investigated. Furthermore, a damage index is developed by using factors related to damage along with a relevant analysis method. A cantilever-type box-type steel member, which is assumed to undergo buckling deformation, is used for the analysis. A nonlinear analysis with repeated displacement control is conducted by applying a compressive load that leads to failure along with a predetermined compressive load to the steel member. The main variables considered in this analysis are the load stock pattern and the type of steel (SS400, SM570, and Posten 80). The influence of each variable on the failure mode, deformation capacity, and damaging process is described. The failure processes for each type of steel are compared. The results indicate that the failure of a steel member under strong repeated loading is governed by local buckling and that the failure of a steel member is directly related to the local strain.

Keywords: *damage index, local stress, local strain, plastic strain under repeated loading*

1. Introduction

Studies on enhancing the strength and usability of steel members for high-rise buildings and long-span bridges have been conducted (Xiong and Liew, 2015; Khan *et al.*, 2015; Mikkola *et al.,* 2015). Furthermore, numerous experiments and numerical analyses of the damage assessment of steel columns, beams, bracings, and other structural members under repeated loading such as an earthquake load have been conducted (Nguyen *et al.,* 2015; Park, 1993; Gao and Usami, 2000).

Owing to the emergence of ultrahigh-strength steels, structural steel shapes are a very important design parameter considering the local buckling, and buckling expressions according to the structural steel shapes and load conditions have been proposed (Seif and Schafer, 2010). In addition, a trilinear kinematic hardening model was proposed to simulate the behavior of ultrahigh-strength steel columns with an H-section under cyclic loading (Wang *et al.*, 2015; Chen *et al.*, 2016).

A steel member that has a low slenderness ratio is less affected by additional flexure owing to the axial force, and lateral buckling is caused by local buckling. Therefore, the local buckling of plate elements is the major reason for failure. According to an experimental study by Park (1993), a steel member accumulates damage during repeated loading, and local buckling leads to buckling of the entire member (Park, 1993). As a very large amount of plastic deformation repetitively occurs in the steel member, the steel member will eventually fracture. It was found that a steel member element can fail when such a large amount of plastic deformation occurs in a steel member element damaged by local buckling, even when the number of repeated loading cycles is low.

In this study, a damage index is developed to quantitatively comprehend the degree of damage due to a large amount of plastic deformation under the repeated loading of steel members. By using this damage index, a method for analyzing the damage to box-type steel members is developed.

2. Damage Assessment

Recently, efforts have been made to comprehend the nonlinear behavioral characteristics of existing buildings constructed without any seismic specifications and to assess their seismic capacity. The use of a damage index to comprehend the degree of damage is gaining popularity. A damage index numerically indicates the degree of damage to structures and members under load and the performance of the member. Further, a damage index uses indicators such as the changes in the natural periodicity of the structure, the changes in strength, a formulation of fatigue, the energy emission of the hysteresis curve (Darwin and Nmai, 1986), and the changes in strain (Stephens and Yao, 1987; Banon *et al*., 1981) to assess the damage to a structure.

2.1 Damage Index of a Member

The damage index developed in the present study is based on the damage index considering the cumulative plastic strain developed by Park (1993) and was derived from the stress–strain

*Member, Professor, Dept. of Civil Engineering at Chonnam National University, Gwangju 61186, Korea (E-mail: parkys@chonnam.ac.kr)
**Member, Ph.D., Examiner at Korea Intellectual Patent Office, Daejeon 35208, Korea (Corresponding Author, E-mail: kkd0724@naver.com)

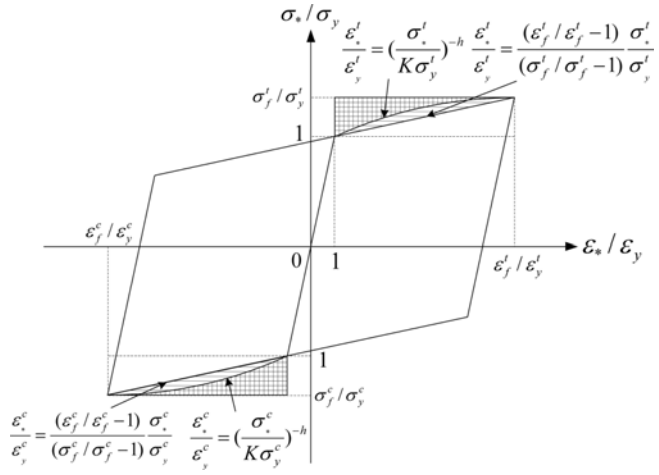

Fig. 1. Dimensionless Local Stress-ratio–strain-ratio Envelope Curve

relationship of a steel member (Park, 1993). The damage to a steel member is defined as the hysteresis of the deformation process, from the initiation of residual deformation to the beginning of failure. The stress–strain relationship was defined to follow a bilinear kinematic hardening hysteresis curve. Furthermore, the degree of damage can be separately assessed by using the plastic strains in the tension and compression zones of the steel member. Thus, the relationship between the dimensionless local stress and strain ratios in the plastic zone can be easily comprehended using a linear equation instead of a higher-order equation, as shown in Fig. 1.

From Fig. 1, the ultimate stress ratio of the most vulnerable element of a steel member under strong and repeated loading is σ_u/σ_y, and the ultimate strain ratio can be expressed as $\varepsilon_u/\varepsilon_y$. Moreover, by using the areal ratio regarding the stress and strain ratios, which represent the cumulative plastic strain in each loading phase and at ultimate loading, the degree of damage to the vulnerable portion can be assessed. Therefore, the damage index D of the vulnerable part of a steel member can be calculated as follows:

$$D = \frac{1}{\alpha}\left(\frac{A_*^t}{A_{limit}^t} + \frac{A_*^c}{A_{limit}^c}\right) \tag{1}$$

$$A_*^t = \int_1^{\sigma_*^t/\sigma_y^t} \frac{(\varepsilon_*^t/\varepsilon_y^t - 1)}{(\sigma_*^t/\sigma_y^t - 1)} \frac{\sigma_*^t}{\sigma_y^t} d\left(\frac{\sigma_*^t}{\sigma_y^t}\right) \tag{2}$$

$$A_*^c = \int_1^{\sigma_*^c/\sigma_y^c} \frac{(\varepsilon_*^c/\varepsilon_y^c - 1)}{(\sigma_*^c/\sigma_y^c - 1)} \frac{\sigma_*^c}{\sigma_y^c} d\left(\frac{\sigma_*^c}{\sigma_y^c}\right) \tag{3}$$

$$A_{limit}^t = \int_1^{\sigma_u^t/\sigma_y^t} \frac{(\varepsilon_u^t/\varepsilon_y^t - 1)}{(\sigma_u^t/\sigma_y^t - 1)} \frac{\sigma_*^t}{\sigma_y^t} d\left(\frac{\sigma_*^t}{\sigma_y^t}\right) \tag{4}$$

$$A_{limit}^c = \int_1^{\sigma_u^c/\sigma_y^c} \frac{(\varepsilon_*^c/\varepsilon_y^c - 1)}{(\sigma_*^c/\sigma_y^c - 1)} \frac{\sigma_*^c}{\sigma_y^c} d\left(\frac{\sigma_*^c}{\sigma_y^c}\right) \tag{5}$$

where A_* is the area of plastic strain in the envelope curve of the local stress and strain ratios in a loading phase, A_{limit} is the limit area of the plastic deformation in the envelope curve of the local stress and strain ratios, the value of the strain constant α is 2 when tensile and compressive strains exist and 1 when either a tensile or compressive strain exists, ε_* is the local strain in a loading phase, σ_* is the local stress in a loading phase, ε_y is the yield strain, σ_y is the yield stress, ε_u is the ultimate strain, σ_u is the ultimate stress, h is the hardening ratio, K is the strength coefficient, and the superscripts t and c denote tension and compression, respectively.

The value of A_{limit} is equal to the area of the plastic strain in the envelope curve when the strain is equal to the ultimate strain in an element. In Eq. (1), when D = 1, failure is initiated in the compression or tension phase. When D < 1, failure has not occurred, but the value of D provides a numerical measure of how much damage has occurred.

Generally, the local strain is more accurately predicted by experimental methods. However, in this study, we present a method for predicting the local strain through an analytical method according to the type of steel by using a commercial nonlinear structural analysis program.

3. Finite-element Analysis for Assessing the Degree of Damage

3.1 Modeling for Nonlinear Analysis

To develop a method for analyzing a steel member under strong and repeated loading and the proposed damage indices, a box-type steel member was used to conduct a nonlinear analysis. Fig. 2 shows the finite-element model and coordinate system of the box-type steel member used for the analysis. In the analysis, a box-type B-100 × 100 × 2.3 model was used, which has one fixed end and one hinged end so that it can freely rotate about the Y axis, which passes vertically through the cross section. The length between the both ends h was set as 480 mm.

In the structural model, quadrilateral elements (QUAD4), which are plate-shell isoparametric elements, were used, and triangular elements (TRIA3) were used around the loading point at the end

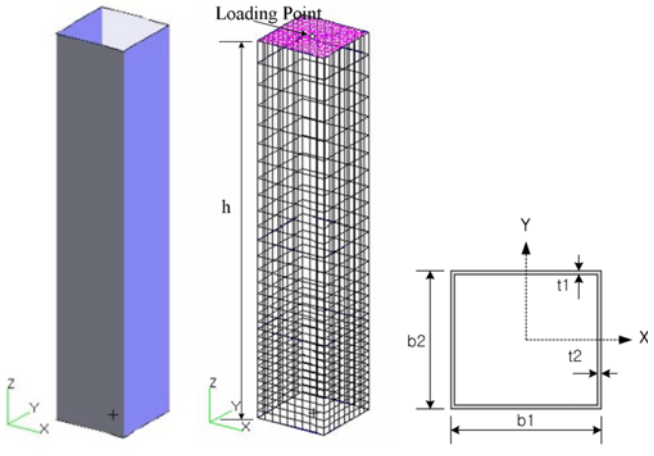

Fig. 2. Analysis Model for the Box-type Steel Member

of the member. An isoparametric element is an element in which the function describing the shape of the element is identical to the displacement function. In this case, the coordinate conversion and displacement function undergo a completely identical conversion. These elements can even be used to model a thick shell. Moreover, regarding the flexure, the stress along the thickness direction is calculated; thus, it can also be applied to a nonlinear member. For QUAD4, the curvature is linearized within the element, and for TRIA3, the strain and curvature are assumed to be identical. An 1116-element model was used in the present analysis, with 31 elements partitioned along the axis of the steel member and 9 elements partitioned along the direction orthogonal to the axis of the steel member (a total of four sides). The division of elements in these models considers the member's deformation such as the overall buckling and local buckling and the correspondence of positions such as the local strain.

In case of a general three-dimensional analysis, the displacement of each joint has six degrees of freedom, whereas in the present rotational restraint analysis, wherein the degree of freedom is not defined for rotation around the tangent of the plate element, each joint was assumed to have five degrees of freedom. In the model shown in Fig. 1, the elastic modulus and yield strength of the part comprising steel blocks are increased so that their behaviors are similar to those of a steel body. The naming convention and parameters for each model are listed in Table 1.

λ is the slenderness ratio of the compressed member and can be calculated using

$$\lambda = \frac{1}{n}\frac{\sqrt{\sigma_y}}{E}\left(\frac{l_e}{r}\right) \tag{6}$$

where E is the Young's modulus, l_e is the effective buckling length, and r is the radius of rotation. R is the equivalent width-to-thickness ratio of the plate element and can be calculated as follows:

$$R = \frac{1}{n}\left(\frac{b}{t}\right)\frac{\sqrt{12(1-\nu^2)}}{k}\frac{\sqrt{F_y}}{E} \tag{7}$$

where t and b are the thickness and width of the plate, respectively, and k is the buckling coefficient.

3.2 Configuration of the Loading Method

First, an analysis of the compressed member that receives the central axial load is conducted. Next, while applying a compressive force of $0.2P_y$ to the joint loading point, the relative displacement of a member along the vertical direction (X axis) in Fig. 1 was given for each phase. The directions in which the displacement, strain, load, and stress are given are set as positive directions. The repeated loading patterns, as shown in Fig. 3, consist of two types: (a) RD type, an alternating gradual increase in loading in the tension and compression zones (by doubling the yield lateral displacement), and (b) CD type, an alternating constant loading in the tension and compression zones (by tripling the yield lateral displacement). The lateral yield displacement was calculated as follows:

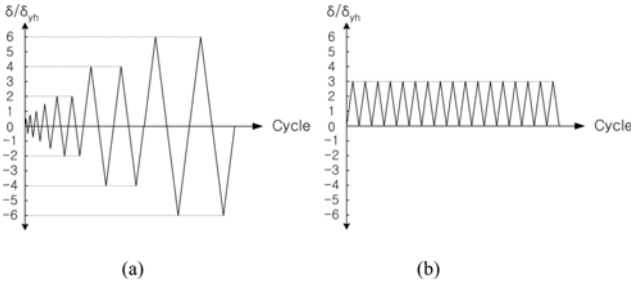

Fig. 3. Loading Patterns: (a) RD Type, (b) CD Type

$$\delta_{yh} = \frac{P_{yh}h^3}{3EI} \tag{8}$$

$$P_{yh} = \frac{M_y}{h} \tag{9}$$

where M_y is the yield moment, and P_{yh} is the lateral yield load.

3.3 Assumptions for the Material Characteristics

The bilinear stress–strain relationship of the kinematic hardening model shown in Fig. 4 was used to describe the material characteristics. The ratio of the gradient E_t of the single-axis stress–strain curve of the plastic zone to the Young's modulus E, the nominal yield stress, the Young's modulus, and the Poisson's ratio are presented in Table 2. Furthermore, the Von Mises yield condition was used. Generally, the analysis precision of the hysteric behavior of a member is largely influenced by the composition of the material. For the analysis of strain hardening, a precise model of the material composition is essential. In this study, the cyclic stress–strain relation in the strain zone was

Table 1. Naming Convention and Parameters for the Model

Length h (mm)	Width $b1$ (mm)	Width $b2$ (mm)	Thickness t; $t1$, $t2$ (mm)	Cross-Sectional Area A (mm^2)	Radius of rotation r (mm)	Width-to-thickness ratio b/t	Slenderness ratio λ
480	100	100	3.2	1239.04	39.54	29.25	24.28

US — 40 — 26 — 56 — CL

(1) (2) (3) (4) (5)

Symbol Description:

(1) Unstiffened Steel Member (3) λ (4) R
(2) Material Type
40: SS400
57: SM570
80: Posten
(5) Loading Pattern
CL: Constant Axial Load
RD: Fully Reversed Displacement Cycles
CD: Constant Displacement Cycles

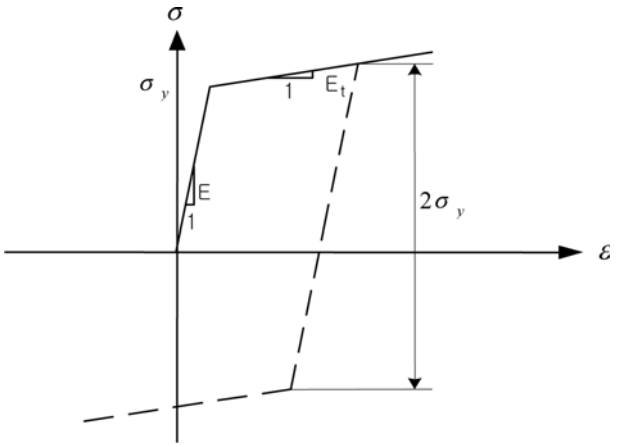

Fig. 4. Stress–strain Relationship Assumed for the Elastoplastic Material

Table 2. Material Characteristics

Name of test subject	σ_y (MPa)	σ_u (MPa)	E_t/E	Material Type
US40-*	235.2	510	24	SS400
US57-*	460.6	597	15	SM570
US80-*	686.0	821	10	Posten 80

Note: E = 205 GPa, v = 0.3, * = including all the supplementary names

investigated. To develop an analysis method using the damage index, the material properties of steel followed a bilinear stress–strain curve.

3.4 Variables of the Analysis

In this study, the analysis was conducted using different types of steel under different loading conditions. The steel types are as follows: SS400, a rolled steel for a general structure; SM570, a rolled steel for a welded structure; and Posten 80, a steel with a high tensile strength. The loading conditions are as follows: CL type, a concentrically compressive load; RD type, an alternating gradual increase in the displacement in the tension and compression zones with a concentrically compressive load of $0.2P_y$; and CD type, an alternating constant displacement with a concentrically compressive load of $0.2P_y$. By conducting a nonlinear analysis using above conditions, the damage process and failure behaviors were compared and analyzed. The specifications are listed in Table 3.

Table 3. Variables of the Analysis

Name of test subject	Material Type	Loading Patten
US40-26-56-CL	SS400	CL
US40-26-56-RD	SS400	RD
US40-26-56-CD	SS400	CD
US57-26-56-CL	SM570	CL
US57-26-56-RD	SM570	RD
US57-26-56-CD	SM570	CD
US80-45-95-CL	Posten80	CL
US80-45-95-RD	Posten80	RD
US80-45-95-CD	Posten80	CD

4. Results and Interpretation

4.1 Steel Members with a Concentrically Compressive Load

The buckling strength of a steel member subjected to a concentrically compressive load rapidly decreases after attaining the maximum value. The major and minor axes of the box-type steel member cannot be distinguished, and its four sides are welded. Therefore, the effect of the compressive residual stress is very large.

The positions of local buckling deformation for test subjects US40-26-56-CL, US57-36-78-CL, and US80-45-95-CL are at 0.146h, 0.125h, and 0.114h, respectively, at the center on the other side of the plane of the buckling direction. This indicates that the position of local buckling deformation decreases as the strength of the steel increases. The analysis results for concentric compression are summarized in Table 4. From the table, the ratio of the strength to the stress for each material subject can be obtained.

The ranges of plastic strain for US57-36-78-CL and US80-45-95-CL are similar. However, for US 40-26-56-CL, the range of plastic strain is 2.53 times lower than that of the others. The local

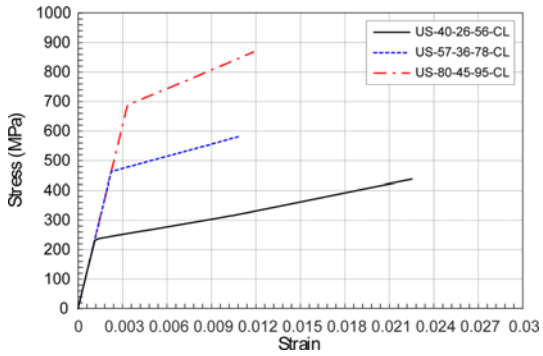

Fig. 5. Local Stress–strain Curves for Each Material Type and Loading Condition (CL)

Table 4. Analysis Results for Concentric Compression

US40-26-56-CL			
Maximum strength P_u (kN)	Yield strength P_y (kN)	Maximum stress σ_{ul} (MPa)	Yield stress σ_{yl} (MPa)
409.32	303.13	437.12	237.16
US57-36-78-CL			
Maximum strength P_u (kN)	Yield strength P_y (kN)	Maximum stress σ_{ul} (MPa)	Yield stress σ_{yl} (MPa)
726.59	578.79	577.22	460.00
US80-45-95-CL			
Maximum strength P_u (kN)	Yield strength P_y (kN)	Maximum stress σ_{ul} (MPa)	Yield stress σ_{yl} (MPa)
927.80	853.47	926.85	686.00

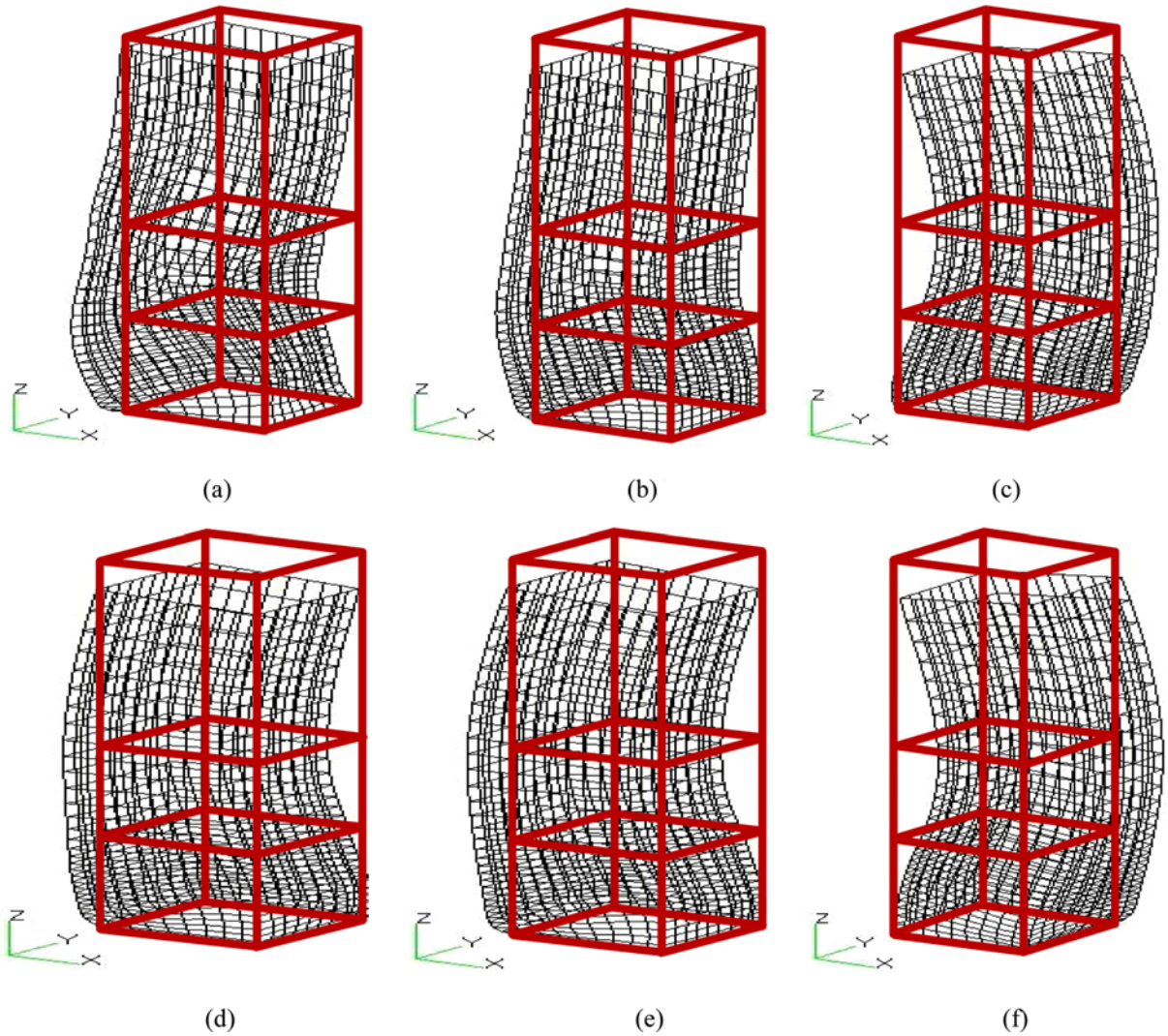

Fig. 6. Deformation of Various Test Subjects Under Various Loading Conditions (RD, CD): (a) US40-26-56-RD, (b) US40-26-56-CD, (c) US57-36-78-RD, (d) US57-36-78-CD, (e) US80-45-95-RD, (f) US80-45-95-CD

stress–strain hysteresis with the most severe stress concentration is shown in Fig. 5.

4.2 Steel Member with an Alternating Displacement

4.2.1 Deformation and Failure of a Member

When gradually increasing the displacement (RD) in the tension and compression zones alternately in the +X direction of the member, local buckling occurs at both the edges of the +X plane, approximately 0.04h right above the fixed end, regardless of the type of steel. This is because the effect of energy diffusion at the fixed end and the buckling strength rapidly decrease owing to repeated deformation and the concentrated residual stress at the edge, where the strength is high.

Figure 6 shows that the deformation under repeated displacement right before the failure of the test subject is 0. For all test subjects, local buckling accompanied overall buckling. Further, buckling did not occur along the entire length for all test subjects but is continuously created from the point at which buckling initiated. As the load increases up to the yield strength, compressive deformation occurs. After exceeding the yield strength, overall buckling occurs. As the load increases, local buckling occurs. The deformation of various tests subjects under different load conditions is shown in Fig. 6.

4.2.2 Hysteric Behaviors of the Local Stress–strain Curves

Each subfigure in Fig. 7 shows the local stress–strain relationship. The stress–strain hysteresis shows the flexural tension and flexural compression of the edge elements around the end where local buckling deformation occurs. Fig. 7(a) shows the hysteresis curves for RD-type loading in the +X plane for each steel type, and Fig. 7(b) show the hysteresis curves for CD-type loading. Fig. 7(c) shows the curves in Figs. 7(a) and 7(b) together. For US40-26-56-RD, the difference in the amplitudes of the compressive strain is 4.49ε_y, and the restoration of the tensile strain under a compressive strain is 93.7%. For US57-36-78-RD,

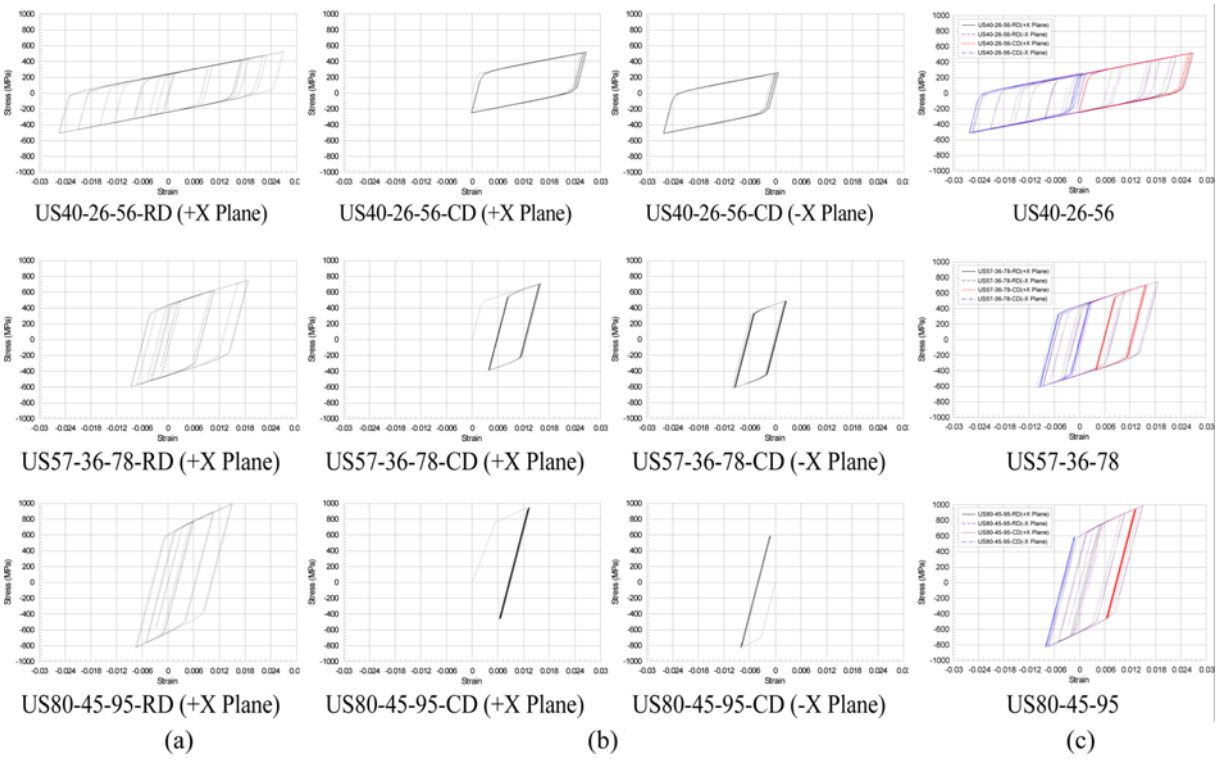

Fig. 7. Local Stress–strain Curve for Various Test Subjects and Loading Conditions (RD, CD): (a) RD Type, (b) CD Type, (c) Overlapping Curves

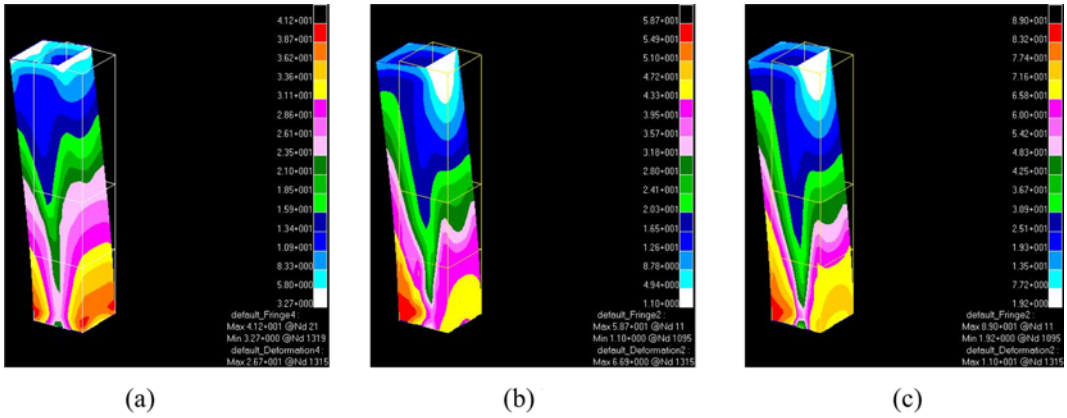

Fig. 8. Stress Distributions of Three Test Subjects (kgf/mm^2): (a) US40-26-56-RD, (b) US57-36-78-RD, (c) US80-45-95-RD

the difference in the amplitudes of the compressive strain is 1.71ε_y, and the restoration of the tensile strain under a compressive strain is 69.6%. Furthermore, for US80-45-95-RD, the difference in the amplitudes of the compressive strain is 2.24ε_y, and the restoration of the tensile strain under a compressive strain is 50.2%. The difference in amplitudes increases by 1.15 times for US57-36-78-RD and 1.51 times for US80-45-95-RD compared to that for US40-26-56-RD. This indicates that the hysteresis of the local strain is more severe in flexural compression. Moreover, it indicates that a higher strength results in more severe compressive deformation. Therefore, it is expected that a crack will be initiated owing to compression under a relatively higher strain, and another crack will be initiated owing to tension.

The strain restoration is 74.3% and 53.6% of that for US40-26-56-RD for US57-36-78-RD and US80-45-95-RD, respectively. In Fig. 7(b), depending on the loading conditions, a compressive strain is only present in the +X plane, and both tensile and compressive strains are present in the –X plane. The –X plane is subjected to a compressive strain, as it is under concentric loading. The strain restoration in the +X plane is 98% for US40-26-56-RD, 76.5% for US57-36-78-RD, and 52% for US80-45-95.

The strain restoration for US57-36-78-RD is 53% of that for US40-26-56-RD. A higher strength results in a more rapid decrease in the plastic strain depending on the period of loading after reaching the ultimate strain. Each subfigure of Fig. 8 shows the stress distributions of three test subjects.

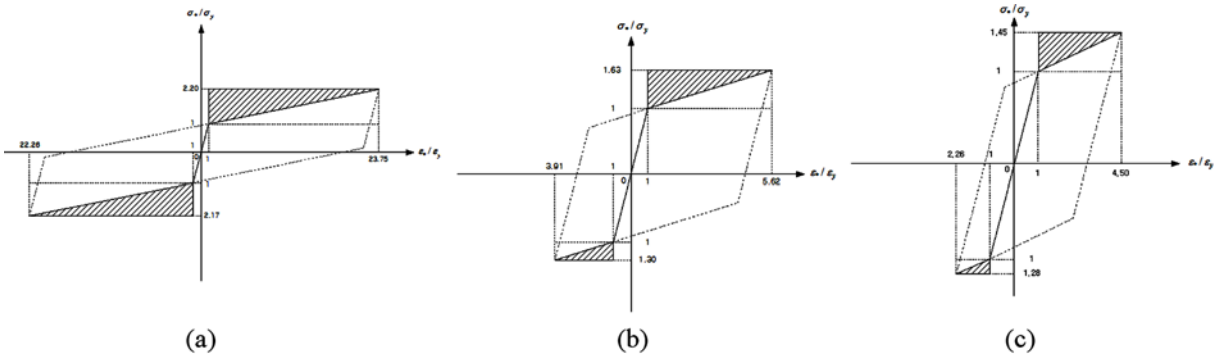

Fig. 9. Dimensionless Local Stress-ratio–strain-ratio Envelope Curves for Various Test Subjects: (a) US40-26-56, (b) US57-36-78, (c) US80-45-95

Table 5. Limit Areas of the Local Stress-ratio–strain-ratio Envelope Curves for Various Test Subjects

Type	US40-26-56	US57-36-78	US80-45-95
$A_{limit}{}^{t}$	24.87	0.87	0.35
$A_{limit}{}^{c}$	27.30	2.91	1.57

4.3 Damage Assessment Using the Damage Index

The limit area of plastic deformation in the envelope curve of the local stress–strain ratio for each test subject (Fig. 9) is listed in Table 5. By using the obtained limit area, the degree of damage to a box-type steel member can be attained. In Fig. 10, the distribution of the damage index for the compression zone of the plane for RD-type loading can be obtained. It is observed that the degree of damage is most severe around the edge near the end. Furthermore, for a test subject with a low strength, the damage is concentrated near the end, and for US40-26-56-RD, almost no damage occurs above 0.5*h*.

As for US80-45-95, a higher strength results in a more uniform range of damage distribution along the height of the steel

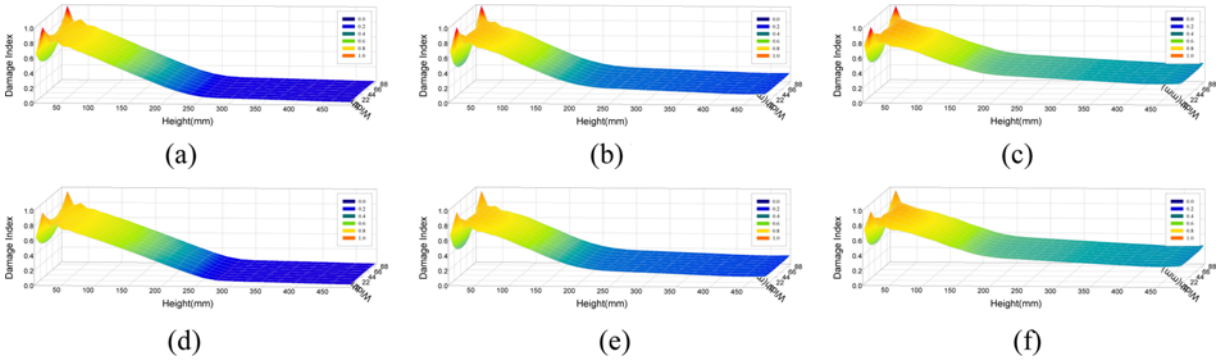

Fig. 10. Distribution of the Damage Index in the Compression Zone of the Plane for Various Test Subjects Under RD-type Loading: (a) US40-26-56-RD (+X Plane), (b) US57-36-78-RD (+X Plane), (c) US80-45-95-RD (+X Plane), (d) US40-26-56-RD (-X Plane), (e) US57-36-78-RD (-X Plane), (f) US80-45-95-RD (-X Plane)

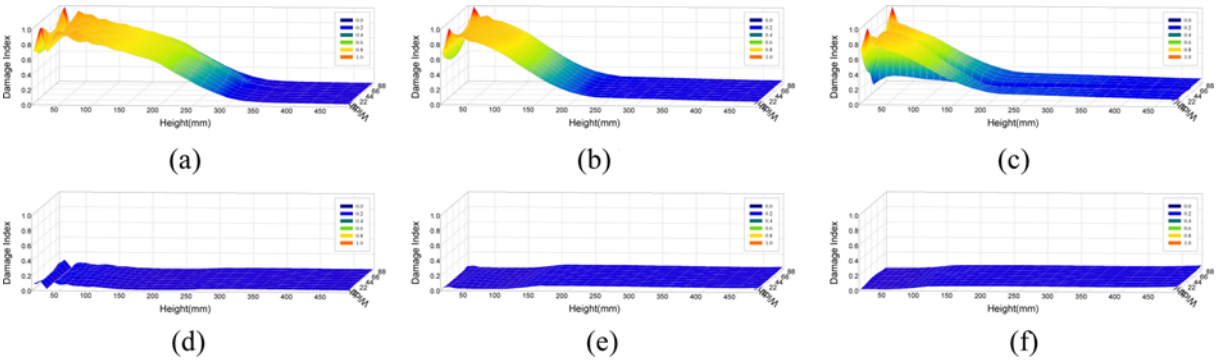

Fig. 11. Distribution of the Damage Index in the Compression Zone of the plane for various subject under CD-type loading: (a) US40-26-56-CD (+X Plane), (b) US57-36-78-CD (+X Plane), (c) US80-45-95-CD (+X Plane), (d) US40-26-56-CD (-X Plane), (e) US57-36-78-CD (-X Plane), (f) US80-45-95-CD (-X Plane)

member. In Fig. 11, the distributions of the damage index for the compression zone of the plane for CD-type loading are shown. Similar to RD-type loading, the degree of damage is most severe around the edge near the end. Unlike RD-type loading, a test subject with a low strength has a wider range of damage. For US40-26-56-RD, the damage reaches a height of 0.63*h*. Moreover, a higher strength results in a more limited range of damage around the end. For US80-45-95-RD, the damage reaches a height of 0.35*h*.

5. Conclusions

The process by which a box-type steel member subjected to strong and repeated loading undergoes failure and the factors relevant to damage were used to develop a new damage assessment method using a nonlinear analysis. The major conclusions of this study are as follows.

1. By using the dimensionless local stress-ratio–strain-ratio envelope curve, a new damage index was proposed. This damage index is an area ratio of the stress ratio and the strain ratio corresponding to the cumulative plastic strain of each load step and the ultimate load state, and the cumulative damage to the member can be taken into account when evaluating the damage capability.
2. The results of a damage assessment using the damage index for a box-type steel member indicated that the position where local buckling occurred was the most severely damaged. This indicates that damage is closely related to the local buckling and plastic strain.
3. The boundary conditions of the model in this study were set as one end fixed and one hinged end. For this reason, local buckling, when occurring concentrically, occurred at lower positions when the strength of the steel member is higher. On the other hand, when repetitive loading is applied, buckling occurred around the edge where stress could be easily concentrated owing to cumulative plastic deformation, regardless of the strength of the steel member.
4. Although the strength of Posten 80, which is the highly tensile, is 1.5 times higher than that of SM 570, the strain restoration of Posten 80 was not lower than that of SM 570.

References

Banon, H., Irvine, H. M., and Biggs, J. M. (1981). "Seismic damage in reinforced concrete frames." *Journal of Structural Division*, Vol. 107, No. 9, pp. 1713-1729.

Chen, S., Chen, X., Wang, Y.-B., Lu, Z., and Li, G.-Q. (2016). "Experimental and numerical investigation of Q690D H-section columns under lateral cyclic loading." *Journal of Constructional Steel Research*, Vol. 121, pp. 268-281, DOI: 10.1016/j.jcsr.2016. 02.015.

Darwin, D. and Nmai, C. K. (1986). "Energy dissipation in RC beams under cyclic load." *Journal of Structural Engineering*, Vol. 112, No. 8, DOI: 10.1061/(ASCE)0733-9445(1986)112:8(1829).

Gao, S., Usami, T., and Ge, H. (2000). "Eccentrically loaded steel columns under cyclic in-plane loading." *Journal of Structural Engineering*, Vol. 126, No. 8, pp. 964-972, DOI: 10.1061/(ASCE)0733-9445 (2000)126:8(964).

Khan, M., Paradowska, A., Uy, B., Mashiri, F., and Tao, Z. (2016). "Residual stresses in high strength steel welded box sections." *Journal of Constructional Steel Research*, Vol. 116, pp. 55-64, DOI: 10.1016/j.jcsr.2015.08.033.

Mikkola, E., Marquis, G., Lehto, P., Remes, H., and Hänninen, H. (2016). "Material characterization of high-frequency mechanical impact (HFMI)-treated high-strength steel." *Materials & Design,* Vol. 89, pp. 205-214, DOI: 10.1016/j.matdes.2015.10.001.

Nguyen, V. B., Mynors, D. J., Wang, C. J., Castellucci, M. A., and English, M. A. (2016). "Analysis and design of cold-formed dimpled steel columns using Finite Element techniques." *Finite Elements in Analysis and Design,* Vol. 108, pp. 22-31, DOI: 10.1016/j.finel. 2015.09.007.

Park, Y.-S. (1993). *Damage Process of Steel Members under Very-Low-Cycle Loading*, Dissertation of Civil Engineering Department, Kyoto University, Kyoto, Japan.

Seif, M. and Schafer, B. W. (2010). "Local buckling of structural steel shapes." *Journal of Constructional Steel Research*, Vol. 66, No. 10, pp. 1232-1247, DOI: 10.1016/j.jcsr.2010.03.015.

Stephens, J. E. and Yao, J. T. P. (1987). "Damage assessment using response measurements." *Journal of Structural Engineering*, Vol. 113, No. 4, DOI: 10.1061/(ASCE)0733-9445(1987)113:4(787).

Wang, Y.-B., Li, G.-Q., Cui, W., Chen S.-W., and Sun, F.-F. (2015). "Experimental investigation and modeling of cyclic behavior of high strength steel." *Journal of Constructional Steel Research*, Vol. 104, pp. 37-48, DOI: 10.1016/j.jcsr.2014.09.009.

Xiong, M. X. and Liew, J. Y. R. (2016). "Mechanical properties of heat-treated high tensile structural steel at elevated temperatures." *Thin-Walled Structures*, Vol. 98, Part A, pp. 169-176, DOI: 10.1016/ j.tws.2015.04.010.